



# The influences of natural structure damage and stress path on mechanical behaviors of soft clay

Zhixin Liang<sup>1</sup> · Hong Sun<sup>1</sup> · Zhaoxing Huang<sup>1</sup> · Fujun Niu<sup>2</sup>

Received: 3 November 2022 / Accepted: 26 April 2023 / Published online: 17 May 2023  
© Springer-Verlag GmbH Germany, part of Springer Nature 2023

## Abstract

This work aims to investigate the influence of structural damage to natural soft clay on its mechanical behavior.  $K_0$  consolidated triaxial tests with loading and unloading stress paths were conducted, and field emission scanning electron microscopy (FESEM) and mercury intrusion porosimetry (MIP) were utilized for microstructural investigation. Macroscopic properties of soil were analyzed by microstructure evolution and damage theory. A pore size distribution index ( $S$ ) was proposed that collectively accounts for the effect of pore size distribution and pore volume. Damage variables were determined based on the  $S$  to evaluate the damage degree of soft clay after  $K_0$  consolidation. The soil structure is obviously damaged when the confining pressure exceeds the preconsolidation pressure (119 kPa), with damage variables reaching 0.5~0.6 between 150 and 250 kPa. The initial tangent modulus and ultimate deviator stress of soft clay by reduced triaxial compression (RTC) tests are lower than those by conventional triaxial compression (CTC) tests. It is associated with relatively different microstructure failure modes, i.e., a loose uniform failure mode for RTC specimens and a locally dense non-uniform failure mode for CTC ones. However, the natural structure is slightly damaged after consolidation, and marginal macro and micro differences were observed between CTC and RTC test results when the confining pressure is less than the preconsolidation pressure. Therefore, the mechanical behavior of soft clay is strongly affected by stress paths and damage to the natural structure during consolidation and shearing processes on the macroscopic and microscopic views.

**Keywords** Soft clay · Microstructure · Stress path · Damage · Mechanical properties

## Introduction

Quaternary soft clay is widely distributed in the Pearl River Delta of China, formed by the geological process of three transgressions and three regressions (Qiao et al. 2021).

With the rapid development of the Hong Kong-Guangdong-Macao Bay Area in recent years, problems such as house cracking, bridge deformation, and tension cracking of underground pipes due to insufficient bearing capacity of soft clay foundations have impeded the progress of society and the economy in turn. Furthermore, hazards caused by poor mechanical deformation properties of soft clay have been widely reported (Cui et al. 2015; Ma et al. 2019; Tan et al. 2020). Consequently, more in-depth and accurate research on the mechanical properties of soft clay is necessary.

The deposit of soft clay has gone through a long geological period, during which specific structure is often formed inside soil by flocculation under certain geographical environments, climates, and other factors. The mechanical behavior of soft clay becomes more challenging to predict due to its natural structure, which threatens engineering construction safety. The viewpoint that soil structure has a significant influence on macroscopic mechanical properties was extensively documented (Akbarimehr et al. 2020; Eslami and Akbarimehr 2021; Gasparre et al. 2011; Li et al.

✉ Hong Sun  
sunhong@sjtu.edu.cn

Zhixin Liang  
lzx2020@sjtu.edu.cn

Zhaoxing Huang  
zhaoxing1995@sjtu.edu.cn

Fujun Niu  
niu fj@scut.edu.cn

<sup>1</sup> State Key Laboratory of Ocean Engineering, School of Naval Architecture, Ocean and Civil Engineering, Shanghai Jiao Tong University, Shanghai 200240, China

<sup>2</sup> Guangdong Provincial Key Laboratory of Modern Civil Engineering Technology, Guangzhou 510641, China

2021; Ng et al. 2020). Study on soil structure has been an important issue, and many puzzles remain unsolved, such as the evolution mechanism of microstructure under different loading conditions and its influence on the macro mechanical behavior of soil. In response to these problems, researchers have made numerous efforts. Nan et al. (2021) performed SEM and MIP tests to study the evolution of microstructure of loess specimens with different structural states before and after consolidated undrained triaxial tests and concluded that the shear properties of natural loess are essentially the result of continuous adjustment of soil microstructure. Zheng et al. (2022) found that the clay pores collapse sequentially from small to large during the one-dimensional consolidation and that the macroscopic deformation was mainly caused by the change of interaggregate porosity. Akbarimehr et al. (2021) investigated the correlation of compression index ( $C_c$ ) between undisturbed and disturbed soil specimens, finding that undisturbed specimens have a smaller compression index due to structural effect, and empirical equations were proposed to predict the  $C_c$ . Gasparre and Coop (2008) conducted a series of oedometer tests introducing a new normalization method to quantify the effect of structure in hard clay during compression. The above shows that the effect of soil structure on consolidation and shear characteristics has been extensively studied as two independent processes.

Varied stress paths frequently lead the soil to exhibit different deformation and strength characteristics. Cai et al. (2018) compared the mechanical behavior of naturally deposited clays under different consolidation stress paths and found that the shear strength of specimens and pore water pressure increased and reduced with increasing the ratio of vertical to horizontal consolidation stresses, respectively. Zhang et al. (2020) carried out a series of consolidated undrained triaxial tests on red clay with different stress paths; the results indicate that the effect of stress paths on cohesion is greater than the internal friction angle, and the shear failure angle of specimens also varies due to different stress paths. In summary, although much literature has been devoted to revealing the mechanical characteristics of soils under various stress paths from macro and micro perspectives, considering the coupling effect of consolidation and shearing, the impact of natural structure damage on the mechanical behavior of soft clay under different stress paths has yet to be investigated from microscopic and macroscopic views.

In order to investigate the influence of the natural structure of soft clay on its mechanical behavior under different stress paths, a series of CTC and RTC tests were carried out. Meanwhile, field emission scanning electron microscopy (FESEM) and mercury intrusion porosimetry (MIP) tests were conducted before and after  $K_0$  consolidation triaxial shearing tests. The macro and micro mechanisms of soft clay are studied by damage theory and fractal geometry method.

## Soil samples and methods

### Soil samples

Soil samples were collected from Fangcun Avenue, Ruyifang, Guangzhou, which lies within longitude  $113^\circ 13'$  and  $40.8''N$  and latitude  $23^\circ 6'$  and  $7.2''E$ , as shown in Fig. 1. Guangzhou is located north of the Pearl River Delta in China, close to the South China Sea, with a wide range of soft clay distribution regions. The soil samples belong to the second layer of the muddy clay, buried at a depth of 3.3–15.5 m and sampled at a depth of 3.3–6.0 m. The undisturbed specimens were taken out using a thin-walled collector and then carefully encapsulated and transported to the laboratory. The static soil pressure coefficient ( $K_0 = 0.65$ ) was obtained from  $K_0$  consolidation tests, and basic physical parameters were measured in the laboratory strictly according to the specification (GB/T 50123–2019), as shown in Table 1. Such soil poses a significant potential hazard to construction safety due to poor physical and mechanical properties, such as high moisture content, large porosity ratio, and high liquid limit. The Casagrande method was used to calculate the preconsolidation pressure  $P_c$  to be 119 kPa based on three sets of oedometer tests.

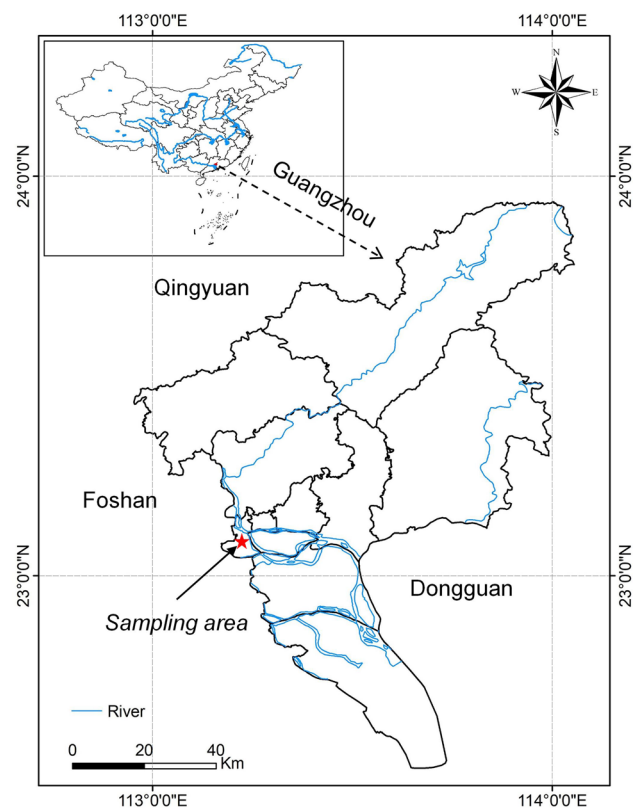


Fig. 1 Location of the sampling site

## Triaxial tests

GDS automatic stress path triaxial apparatus (GDSTTS40, UK) was employed to conduct a series of consolidated undrained (CU) triaxial tests. Natural soft clay specimens were fixed on a soil cutter and carefully cut into cylinders of 80 mm height and 39.1 mm diameter and then tested at four different confining pressures, i.e., 50 kPa, 100 kPa, 150 kPa, and 200 kPa. The following are the specific steps. (1) Back pressure saturation: the specimen was saturated by linearly increasing the confining and back pressure simultaneously with specimen drainage valves opened. Take the Skempton coefficient  $B$  value greater than 0.95 as the judgment basis for saturation completion. (2)  $K_0$  consolidation: the implementation of  $K_0$  consolidation was based on the volume strain during consolidation being the same as the product of the axial strain and the initial cross-sectional area of specimens. The stress path triaxial apparatus realizes the above process by servo control of the confining pressure, ensuring specimens from lateral deformation. The stress loading rate in this process must be slow enough to prevent the generation of excess pore water pressure for accuracy. So, the loading rate was taken as 0.2 kPa/min in this test. (3) Triaxial loading: after consolidation, the drain valve was closed for undrained shearing. The stress-controlled loading was adopted, with a shear rate of 0.2 kPa/min, and the axial strain of 15% was considered the shear failure. Two loading stress paths were used in this test, i.e., conventional triaxial compression (CTC) and reduced triaxial compression (RTC), which was also the most common stress path of foundation soil during engineering construction, as shown in Fig. 2.

## Soil microstructure tests

FESEM and MIP tests were performed on undisturbed specimens as well as the specimens after  $K_0$  consolidation and shear failure. Note that the specimens generated relatively homogeneous deformation during triaxial loading, i.e., no shear band or obvious bulge appears. A field emission scanning electron microscope (MIRA3) produced by TESCAN company with a resolution of 1.2 nm (15 kV) was used. The

scanning plane parallel to the loading direction was chosen to observe the evolution characteristics of the microstructure. Firstly, 10 mm × 15 mm × 10 mm cuboid subspecimens were cut carefully in the center of the specimen using a small wire saw coated in petroleum jelly. The subspecimens were immersed in liquid nitrogen and rapidly cooled to − 196 °C for 30 min and then put in a freeze-dryer for 24 h to allow the moisture to evaporate fully while ensuring that the drying process did not cause soil structure disturbance. After that, the dried specimen was first broken off in the middle, and the floating dust on the section was gently blown away with a washing ear ball. Then ion sputtering was performed on the specimen to increase its conductivity and finally placed in the vacuum chamber of the electron microscope for scanning. Multi-point scanning ensured that the quantitative processing results were statistically significant. Scanning magnifications of 2000× and 10,000× were used for qualitative and quantitative analysis of soil microstructure.

The automatic mercury porosimeter (AutoPoreIV9500) of the American Micromeritics Instrument Corporation was utilized for MIP tests, and it can measure pore sizes ranging from 0.003 μm to 1100 μm. The MIP test is based on the principle that non-wetting liquid does not permeate solid pores without applying pressure. The information of pore size in soil can be derived using the Washburn equation (Washburn 1921) by gradually increasing pressure

$$d = \frac{-4T_s \cos\theta}{p} \quad (1)$$

where  $d$  is the pore diameter,  $p$  is the absolute pressure,  $\theta$  is the indirect contact angle between mercury and soil, and  $T_s$  is the surface tension of mercury. In this research,  $\theta = 130^\circ$  and  $T_s = 0.485$  N/m were employed (Sun et al. 2020; Wang et al. 2020). In order to minimize the disturbance to the microstructure during the mercury intrusion pores, the low-pressure unit (0.52–30 psia) and high-pressure unit (30–60,000 psia) were used to apply pressure step by step in 52 steps (Jiang et al. 2014). The corresponding pore diameter at 0.52 psia is 347 μm and 3 nm at 60,000 psia, so the measurement range of pore size is 3 nm ~ 347 μm. The specific test procedure is shown in Table 2.

## Test results

### Microstructure evolution before and after the $K_0$ consolidation

Figure 3 presents the FESEM image of the natural soil. It can be found that the soil particles stick together, forming large aggregates with various structural forms, as shown in the rectangular box in Fig. 3b. These aggregates are

**Table 1** Physical parameters of natural soft clay

| Property                             | Value |
|--------------------------------------|-------|
| Natural density (g/cm <sup>3</sup> ) | 1.68  |
| Natural water content (%)            | 57.0  |
| Specific gravity                     | 2.70  |
| Liquid limit (%)                     | 59.7  |
| Plastic limit (%)                    | 24.0  |
| Void ratio                           | 1.52  |

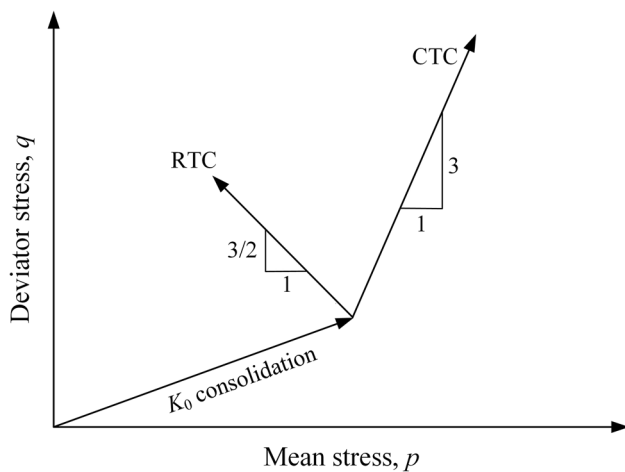


Fig. 2 Stress paths of triaxial tests in this study

flocculent or clotted, constituting the soil skeleton; many pores of different sizes are distributed randomly among soil particles, forming an open structure. Figure 4 shows 10,000 × magnification FESEM images of the soft clay after  $K_0$  consolidation at various confining pressures. When the confining pressure is 50 kPa and 100 kPa, the soil aggregates are still considerable, and particle fragmentation is not visible compared to the natural specimen. Nevertheless, as the confining pressure rises above the preconsolidation pressure, i.e., when it reaches 150 kPa or 200 kPa, large aggregates disintegrate gradually, and many small soil particles appear. These small particles are mainly flaky with irregular edge profiles whose arrangement is chaotic. Most soil particles are in face-to-face and edge-to-face contact, where the former contact form is the most common. According to these characteristics, it can be preliminarily judged that the natural structure of soil has been damaged to a certain extent and has experienced structural reorganization, gradually transforming from a flocculent structure to a dispersed structure. Because FESEM images only reflect scanning plane information qualitatively, it is necessary to propose a structural parameter to more accurately characterize the degree of damage to the natural structure of soft clay after  $K_0$  consolidation under different confining pressures.

Figure 5 presents the pore size distribution curve of natural soft clay. The curve is unimodal with a dominant pore distribution interval of  $0.02 \mu\text{m} \sim 2 \mu\text{m}$ , in which the pore content accounts for 94.9% of the total content. The dominant pore size is  $0.678 \mu\text{m}$  with a content of 0.059 ml/g. Intuitively, as shown in Fig. 6, the pore size distribution curve shifts to the left accompanied by decreased peak value with increasing consolidation pressure, implying that the large pore is gradually compressed. Furthermore, this trend becomes more pronounced when the confining pressure exceeds the preconsolidation pressure. The change of pore number or volume with different sizes can reflect the change in soil microstructure. Also, describing the variation in internal structure state by the change in pore space is a very effective method (Delage 2010; Li et al. 2020a, b; Wang and Xu 2007). However, the conventional pore ratio concept can only be used to characterize the global pore volume effect but does not reflect the effect of pore size distribution. Combining the pore size distribution with the pore volume allows a relatively complete description of the soil structure state from a pore perspective. Accordingly, the pore size distribution index  $S$ , denoting the area enclosed by the pore size distribution curve and the horizontal coordinate axis, was proposed here to characterize pore changes. Based on the idea of calculating area by the trapezoidal method in calculus theory and combined with the pore size distribution characteristic of soil, the pore size distribution index  $S$  is given by

$$S = \sum_{i=1}^{n-1} (d_{i+1} - d_i) \times \frac{(V_i + V_{i+1})}{2} \tag{2}$$

where  $d_i$  and  $V_i$  are the diameter and volume of the  $i$ th pore group, respectively;  $n$  is the total number of pore groups. As shown in Fig. 5,  $(d_{i+1} - d_i)$  represents the difference in pore sizes of adjacent pore groups, and  $(V_i + V_{i+1})/2$  refers to the average volume of these two pore groups. It is not difficult to imagine that a more homogeneous soil structure and smaller total pore volume will result in a smaller  $S$  value. Since the inclusion of individual oversized pores in the calculation will generate significant discrete errors and these pores have minimal content (less than 3%), they will be discarded. Consequently, the pores with a diameter of fewer than  $60 \mu\text{m}$  were selected for calculation. Compared

Table 2 Test scheme

| Test type           | Confining pressure (kPa)     | $K_0$ | Stress path                          | Shear rate  | FESEM test | MIP test |
|---------------------|------------------------------|-------|--------------------------------------|-------------|------------|----------|
| $K_0$ consolidation | 50, 100, 150, 200, 250, 1600 | 0.65  | /                                    | /           | Yes        | Yes      |
| CTC                 | 50, 100, 150, 200            |       | $\Delta\sigma_3=0, \Delta\sigma_1>0$ | 0.2 kPa/min | Yes        | Yes      |
| RTC                 | 50, 100, 150, 200            |       | $\Delta\sigma_3<0, \Delta\sigma_1=0$ | 0.2 kPa/min | Yes        | Yes      |

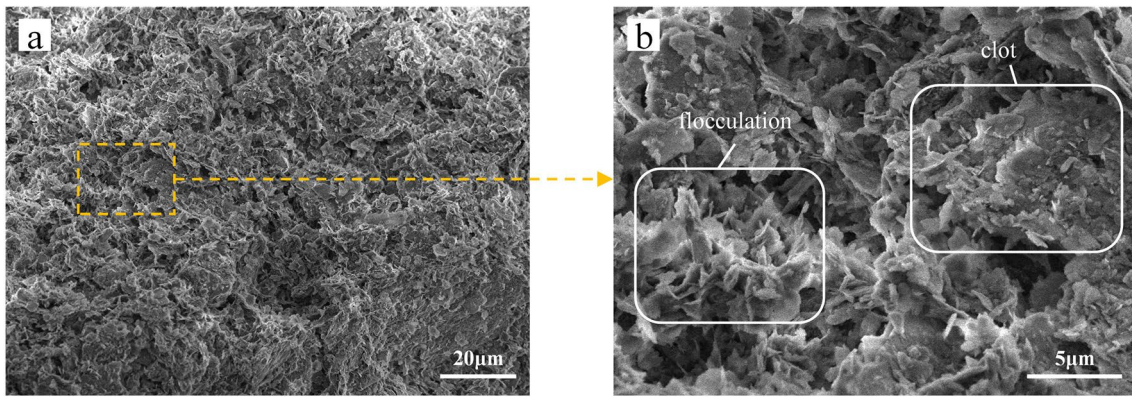


Fig. 3 FESEM images of the specimen at the natural state: a 2000× magnification; b 10,000× magnification

with modified probability entropy (Ren et al. 2022), which quantifies the arrangement of pores or particles, the pore size distribution index reflects the size distribution and volume characteristics of pore populations. This new parameter may be used for developing advanced constitutive models incorporating microstructure characteristics which many scholars

have been studying (He et al. 2022; Liu et al. 2022; Musso et al. 2020).

According to the classical damage theory, the damage variable  $D$  is utilized here to characterize the damage degree to the natural structure of soil after  $K_0$  consolidation. Because the  $S$  could describe the internal structural

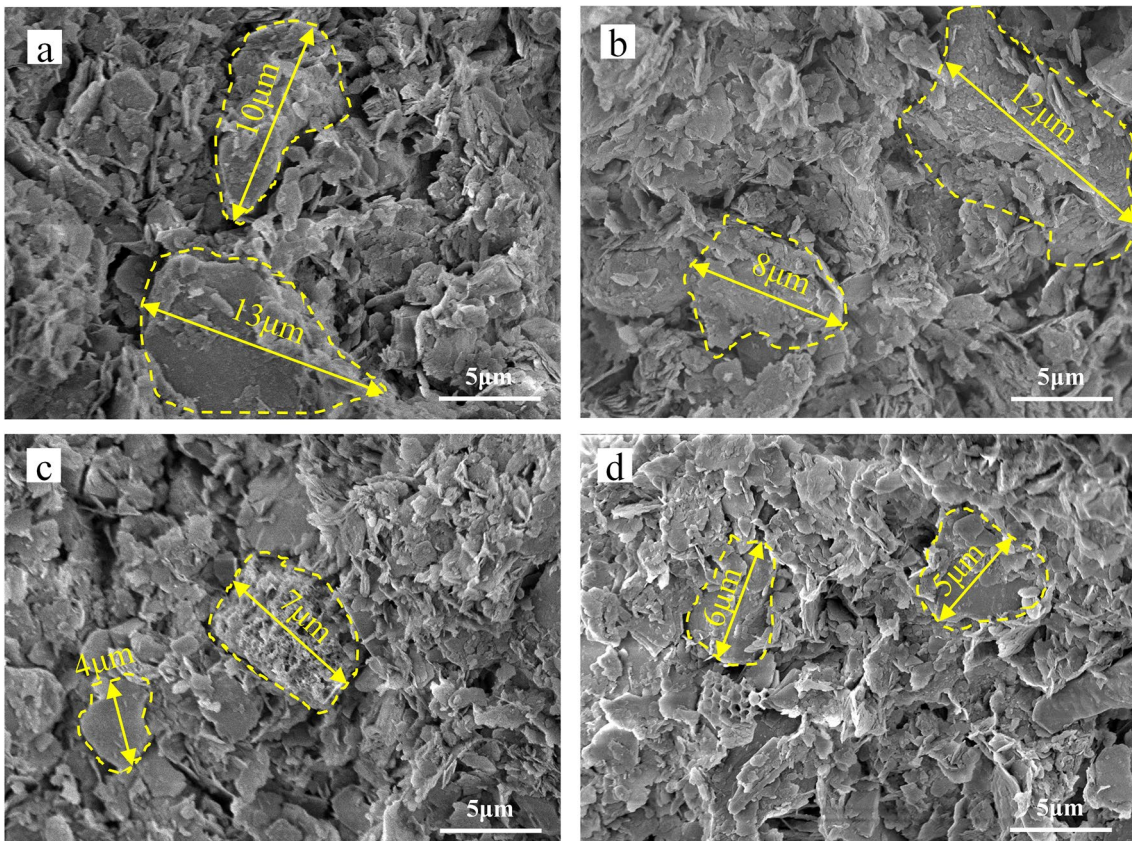


Fig. 4 Micrographs of specimens after  $K_0$  consolidation at various confining pressures: a  $\sigma_3=50$  kPa; b  $\sigma_3=100$  kPa; c  $\sigma_3=150$  kPa; d  $\sigma_3=200$  kPa

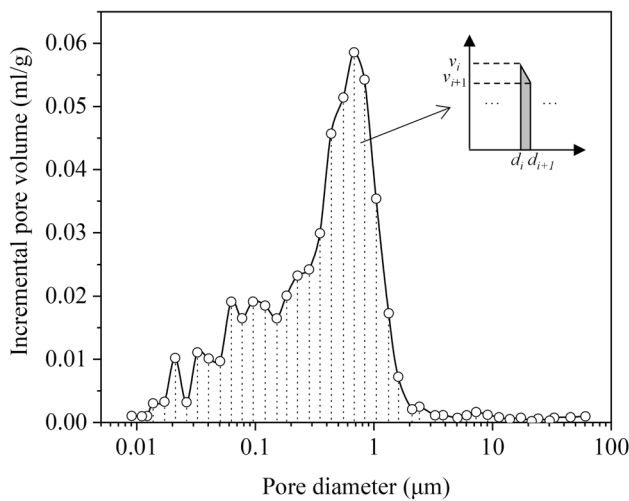


Fig. 5 Pore size distribution of natural soft clay

states of soil and show a sensitive variation with stress, the damage variable is therefore defined as follows:

$$D = \frac{S_{c0} - S_{c1}}{S_{c0} - S_{c2}} \quad (3)$$

where  $S_{c0}$  and  $S_{c1}$  represent the pore distribution index of the natural specimen and after consolidation at a given confining pressure, respectively, and  $S_{c2}$  is the value after consolidation at 1600 kPa. The following is an explanation of the determination of  $S_{c2}$ . According to numerous consolidation test results (Low and Phoon 2008; Ovando Shelley et al. 2020; Xu and Coop 2016; Zeng et al. 2022), the  $e$ -log  $p$  curves of the undisturbed and the remolded clay specimens show almost the same slope when the consolidation pressure

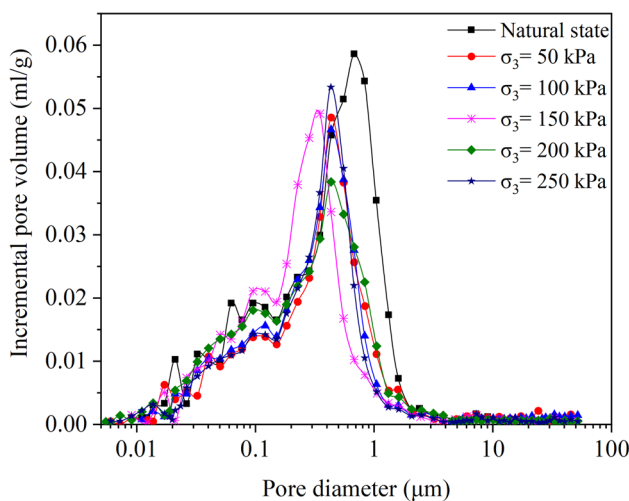


Fig. 6 Pore size distribution after  $K_0$  consolidation under different confining pressures

is up to about 1600 kPa. It indicates that the two specimens generate nearly identical strain under the same load increment. Consequently, it is considered that the natural structure of the soil has been destroyed. Based on this, a MIP test was performed on the soil specimen after consolidation at 1600 kPa as a reference and calculated the corresponding pore distribution index to be  $S_{c2}$ .

$D$  between 0 and 1,  $D$  equal to 0 and 1 represents that the natural structure of soils is intact and completely damaged, respectively. The relationship between damage variables and confining pressures was plotted in Fig. 7. When the confining pressure is less than the preconsolidation pressure (119 kPa), the natural structure is slightly damaged, with the  $D$  value being close to 0. However, the damage variable reaches 0.5~0.6 when the confining pressure ranges from 150 to 250 kPa, which indicates that the structural strength of soils is insufficient to resist the external load and noticeable damage occurred. According to the above discussion, the method for determining damage variables can be considered reasonable.

### Microstructure characteristics subjected to different stress paths

#### Pore size distribution

Researchers have proposed various approaches for classifying soil pores in previous studies (Lei et al. 2020; Lei 1988; Wang et al. 2021a). In this research, the surface fractal model (Korvin 1992; Romero and Simms 2008; Sun et al. 2020) was utilized to categorize pores to investigate the variation of the pore size content of each component under different confining pressure and stress paths. The surface fractal dimension calculation expression is as follows:

$$\log[(dV_p/dV_{max})/d_p] \propto (D_s - 4) \log p \quad (4)$$

where  $p$  is the intrusion pressure of mercury at a certain level,  $V_p$  is the corresponding cumulative intrusion volume when the pressure is  $p$ ,  $V_{max}$  is the total volume of mercury intrusion, and  $D_s$  is the surface fractal dimension. The MIP data of CTC and RTC tests at the confining pressure of 50 kPa was taken as the benchmark, and the  $\log[(dV_p/dV_{max})/d_p] - \log p$  scatter plot was established. As shown in Fig. 8, pores exhibit apparent self-similarity and multiple fractal characteristics. So then, based on the value of the pore diameter at the inflection point position in the scatter plot, the pore size is split into three intervals: small pores ( $< 0.5 \mu\text{m}$ ), mesopores ( $0.5 \sim 5 \mu\text{m}$ ), and macropores ( $> 5 \mu\text{m}$ ). From this, the pore content of each component after CU triaxial tests under different confining pressures and stress paths can be obtained, as shown in Table 3.

Figure 9 presents the pore size distribution of CTC and RTC tests under various confining pressure. Under CTC paths, when the confining pressure is less than the preconsolidation pressure (119 kPa), the content of small pores is dominant, reaching 74.38% and 83.48% of the total pore content, respectively, and the content of mesopore and macropore is low relatively. However, the content of small pores decreases by 15% ~ 20% on average when the confining pressure increases to 150 kPa and 200 kPa, leading to the corresponding rise in mesopore and macropore. As shown in Table 3, the pore content of each component does not differ much from 50 to 100 kPa for RTC tests, after which the content of small pores increases, accompanied by a decreasing mesopore content. The above suggests that the evolution of pore size distribution varies with stress paths and confining pressure. For CTC tests, when the confining pressure exceeds the preconsolidation pressure of soil, the content of small pores decreases, and the content of mesopore and macropore increases. In contrast, the evolution pattern of pore size distribution in RTC tests exhibits a rise in small pore content and a corresponding decrease in mesopore and macropore content.

To compare the evolution characteristics of pores after CTC and RTC tests in the same initial structural state, the pore size distribution curves were plotted as shown in Fig. 10. Figure 10a shows the pore size distribution after CU triaxial tests when the natural structure of soils is slightly damaged before shearing. One can see that the shape of the pore size distribution curves of two stress paths at confining pressures of 50 kPa and 100 kPa is similar. Specifically, the pore size distribution curves all reveal a high peak type with obvious peak points at 50 kPa and a low peak type without clear peak points at

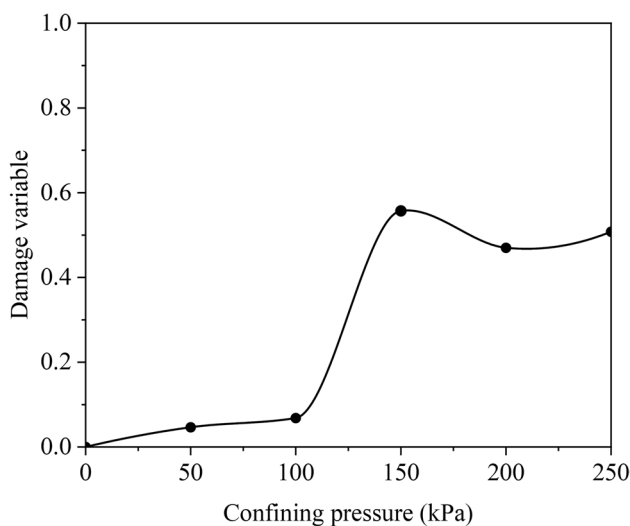


Fig. 7 Relationship between damage variable and confining pressure

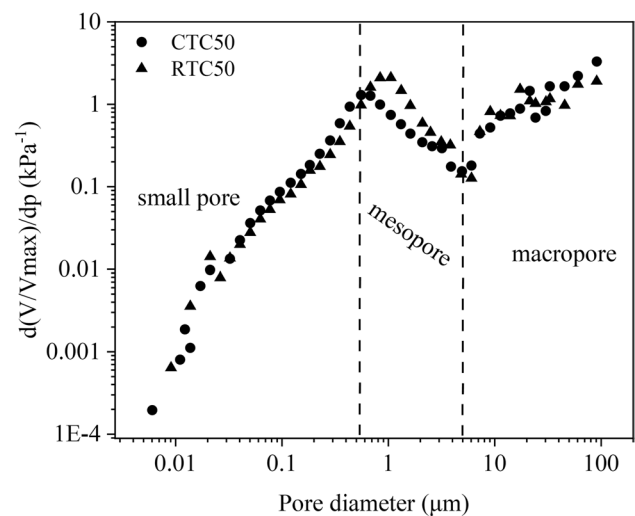
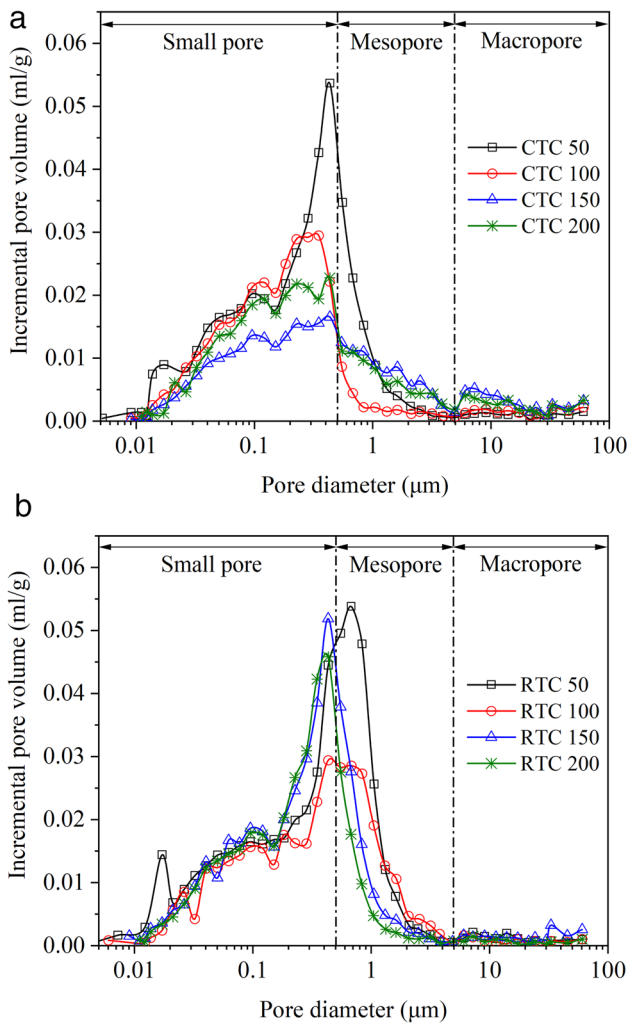


Fig. 8 Fractal characteristics of pores

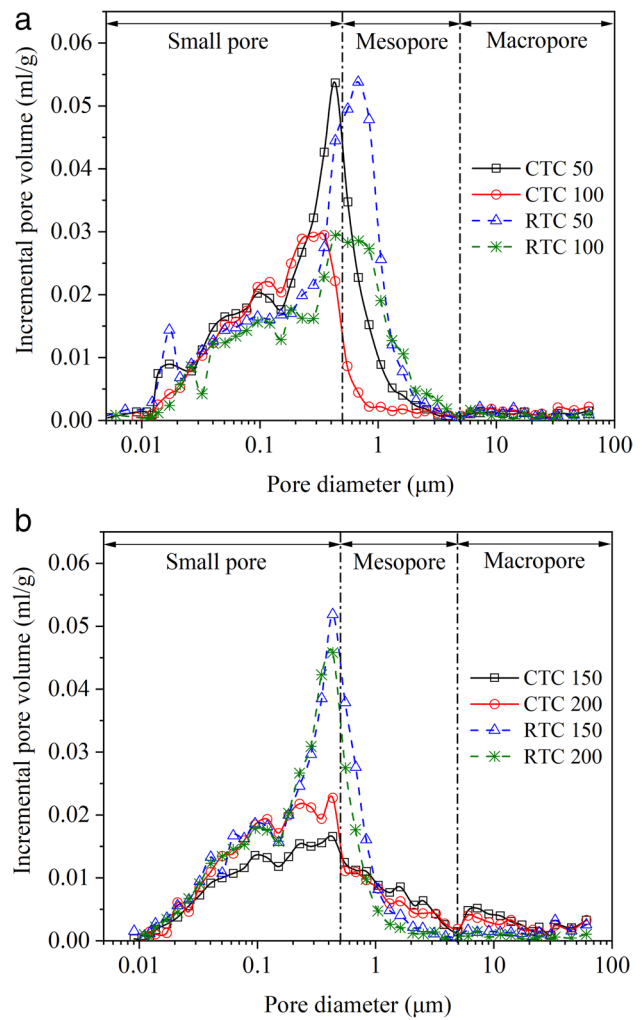
100 kPa; the difference is that compared with the CTC path, the curve of the RTC path moves to the left as a whole. The pore diameter at the peak point of CTC 50 and RTC 50 is 0.434 μm and 0.678 μm, respectively. However, the pore evolution pattern under different stress paths shows considerable differences when the natural structure is strongly damaged during consolidation. The pore size distribution curves of CTC and RTC tests at 150 kPa and 200 kPa exhibit some self-similarity. The positions and shapes of the curves are relatively close under the respective stress paths despite the different confining pressures, especially in CTC tests, as shown in Fig. 10b. It is worth noting that the content of medium to large pores in the CTC test is higher than that in the RTC test, which is different from the pore size distribution pattern when the initial structure of the soil remains relatively intact.

Table 3 Pore content of each component after CU triaxial tests

| Experimental type | Pore volume percentage |                          |                    |
|-------------------|------------------------|--------------------------|--------------------|
|                   | Small pore (<0.5 μm)   | Mesopore (0.5 μm ~ 5 μm) | Macropore (> 5 μm) |
| CTC 50            | 74.38%                 | 21.21%                   | 4.41%              |
| CTC 100           | 83.48%                 | 7.29%                    | 9.23%              |
| CTC 150           | 54.77%                 | 26.94%                   | 18.29%             |
| CTC 200           | 68.20%                 | 20.06%                   | 11.74%             |
| RTC 50            | 55.75%                 | 40.41%                   | 3.84%              |
| RTC 100           | 57.81%                 | 36.66%                   | 5.53%              |
| RTC 150           | 69.17%                 | 23.82%                   | 7.01%              |
| RTC 200           | 78.22%                 | 17.83%                   | 3.95%              |



**Fig. 9** Pore size distributions of specimens after different CU triaxial tests: **a** after CTC tests; **b** after RTC tests



**Fig. 10** Pore size distributions of specimens after different CU triaxial tests: **a**  $\sigma_3 = 50, 100$  kPa; **b**  $\sigma_3 = 150, 200$  kPa

**Structure factor *R***

Pore size distribution index *S* is a powerful parameter to describe the microstructure properties of soil. The damage variable defined based on *S* has well characterized the structural damage of soft clay after consolidation. Consequently, the structure factor *R* is proposed here based on pore size distribution indexes to describe the structural characteristics of soil after shearing. *R* can be expressed as

$$R = \frac{S_{t1} - S_{c1}}{S_{c1}} \tag{5}$$

where  $S_{c1}$  and  $S_{t1}$  are the pore size distribution index of specimens before shearing (after the consolidation) and after shearing, respectively. In the process of undrained shearing, the total pore volume in specimens remains unchanged

from the end of consolidation to shearing failure, only the interconversion between pores of different sizes. As a result, the increasing *R* value suggests the rise of larger pore content, meaning the number of pores is reduced and poor pore dispersion. On the contrary, with a constant total volume of pores, the less the content of larger pores, the greater the number of pores will be; thus, a weaker overall linkage between soil particles appears, resulting in poorer mechanical properties such as lower strength and stiffness.

The structure factors for different stress paths and confining pressures are presented in Fig. 11. At the confining pressures of 50 kPa and 100 kPa, the *R* values of the two stress paths are slightly different. However, when the confining pressure rises to 150 kPa and 200 kPa, the structure factor of CTC tests is significantly larger than that of RTC tests. Specifically, under 50 kPa and 100 kPa confining pressure, the difference in structure factor between the two paths is 0.1~0.2, while it reaches 0.6~1.1 when the confining



pressure rises to 150 kPa and 200 kPa. This illustrates that a significant difference in pore structure arises under high confining pressure. There are more dispersed pore space distribution and looser soil particles in specimens of RTC tests compared to those of CTC tests. Therefore, the microstructural evolution pattern subjected to stress paths is closely associated with the natural structure state.

### Fractal dimension based on FESEM images

Fractal geometry approaches have been widely used in microstructure analysis of geotechnical materials due to the complexity of pore and particle geometry inside the soil. Many fractal dimension calculation methods based on SEM images have been employed to analyze the soil microstructure (Du et al. 2022; Liu et al. 2020; Zheng et al. 2021), among which the box counting dimension is one of the most effective methods. The grayscale image is converted to a binary image using the global threshold segmentation approach, with the optimal threshold for image segmentation being approximately 80% of the peak gray level. The white and black areas represent pores and particles, respectively. As shown in Fig. 12, the binary image is divided by a square grid with side length  $\epsilon$ , the number of pores contained in the grid is  $N(\epsilon)$ , and if the value of  $\epsilon$  is changed,  $N(\epsilon)$  will also change. So, a series of values of  $\epsilon$ ,  $N(\epsilon)$  can be obtained and plotted in a double logarithmic coordinate system, and then, the fractal dimension  $D_f$  can be expressed as

$$D_f = -\lim_{\epsilon \rightarrow 0} \frac{\ln N(\epsilon)}{\ln(\epsilon)} \tag{6}$$

During the shear process of CU triaxial tests, the total volume of pores in the soil specimen remains constant, as mentioned above. The bigger  $D_f$  indicates a greater number of pores and a more dispersed distribution, which signals more serious particle fragmentation. As a result, the fractal dimension of pores is an effective measure for describing soil particle fragmentation. The more broken the soil particles are, the worse the mechanical properties of specimens will be during the loading process. Specifically, the segmented binary image was first imported into MATLAB, and then, the fractal dimension was calculated using the free toolbox FracLab. For each level of confining pressure, multiple FESEM images at different scanning positions were used for analysis and calculation. The average value was taken as the final fractal dimension to make the data statistically meaningful.

As shown in Fig. 13, the fractal dimension of pores after CTC and RTC tests is 1.602 and 1.612 at 50 kPa confining pressure, respectively, and 1.632 and 1.630 at 100 kPa confining pressure, respectively, with less variance under different stress paths at the same confining pressure. However,

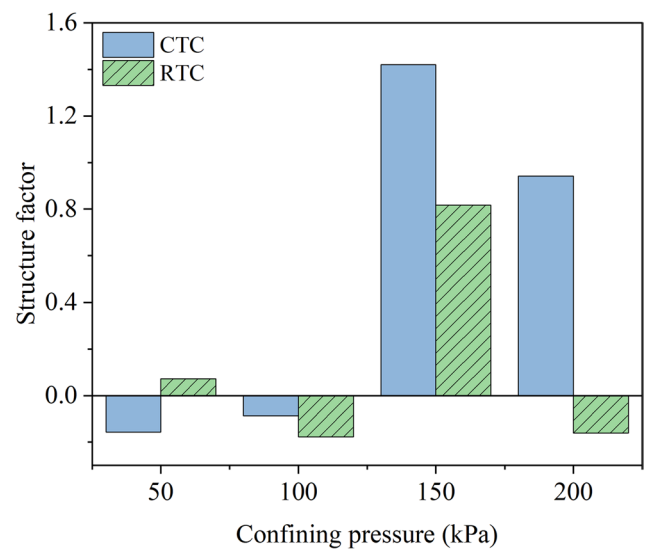


Fig. 11 The relationship between structure factor and confining pressure

as the confining pressure increases further, the difference in the fractal dimension of both stress paths becomes more apparent. For CTC tests, the fractal dimensions at the confining pressures of 150 kPa and 200 kPa are 1.621 and 1.633 respectively, and 1.662 and 1.681, respectively for the RTC tests. Also, the fractal dimension of RTC 150 is 2.53% greater than that of CTC 150, and RTC 200's fractal dimension is 2.94% larger than that of CTC 200. It illustrates that the fractal characteristic of pores is impacted by natural structure. In summary, the soil aggregates are more fragmented, and the soil structure is looser after RTC tests than those after CTC tests at high confining pressure, which is also consistent with the result shown in structure factors.

## Discussion

### Correlation between microstructure and macroscopic mechanical behaviors

Deviator stress–strain curves of soft clay under various confining pressures and stress paths are shown in Fig. 14. The curves for different stress paths all exhibit a weak strain-hardening type. Stress–strain curves move upward as increasing confining pressure, signifying an increase in soil strength. In addition, at 50 kPa and 100 kPa confining pressure, CTC and RTC tests exhibit a similar stress–strain relationship under the same confining pressure. Nevertheless, the stress–strain characteristics of the two stress paths appear clear distinctions with the increase of the confining pressure further. The soil strength of CTC tests is gradually higher than that of RTC tests when the confining pressure reaches

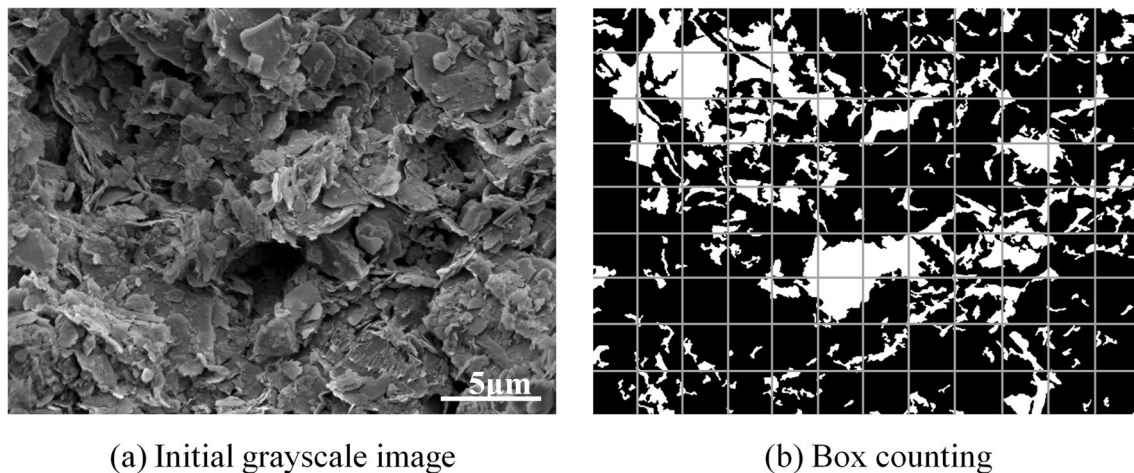


**Fig. 12** Box counting dimension acquisition method

150 kPa and 200 kPa. According to the hyperbolic model proposed by Kondner (1963), the initial tangent modulus  $E_i$  and ultimate deviator stress  $(\sigma_1 - \sigma_3)_{ult}$  can be obtained. As seen from Fig. 15, the ultimate deviator stress of CTC and RTC tests is almost equal when the confining pressure is 50 kPa and 100 kPa, and their initial tangent modulus is also not much different. However, as the confining pressure increases beyond the preconsolidation pressure,  $E_i$  and  $(\sigma_1 - \sigma_3)_{ult}$  under CTC paths are gradually larger than those under RTC paths, which can be seen to be particularly obvious at 200 kPa confining pressure, where the  $(\sigma_1 - \sigma_3)_{ult}$  and  $E_i$  of CTC 200 are 19.5% and 75.0% higher than those of RTC 200, respectively.

Figure 15 also shows that the macroscopic mechanical parameters of the soil are closely related to structure factors. Specifically, when the confining pressure is less than the

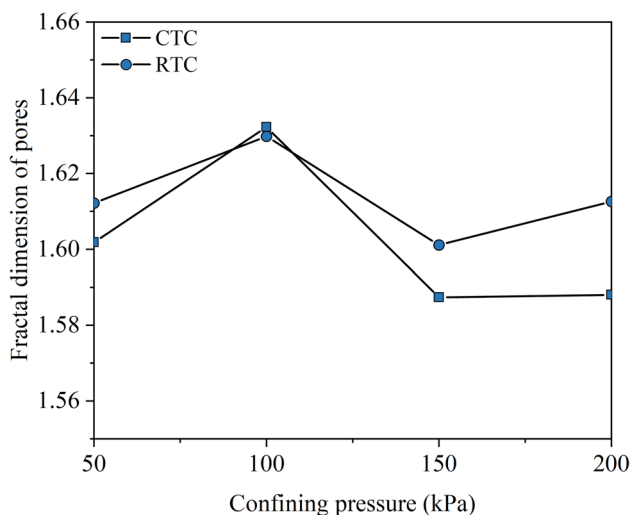


**Fig. 13** Fractal dimension of pores after CU triaxial tests

preconsolidation pressure, the difference in structure factors of the two stress paths is only 0.23 ( $\sigma_3 = 50$  kPa) and 0.09 ( $\sigma_3 = 100$  kPa); thus, the corresponding initial tangent modulus and ultimate deviator stress are also not much different. However, the structure factor of CTC specimens is 0.6 and 1.1 higher than that of RTC ones when the confining pressure reaches 150 kPa and 200 kPa, and the corresponding initial tangent modulus is 40% and 75% higher, respectively. Likewise, the fractal dimension of pores has a similar relationship with the above mechanical parameters, with no specific description here for simplicity. To sum up, there is a close correlation between the evolution characteristics of microstructure (including pore size distribution, structure factor, and fractal dimension) and macro mechanical properties. The microstructure change is the underlying reason responsible for the different mechanical behavior of soils (Guglielmi et al. 2022; Yin and Vanapalli 2022; Zhang et al. 2023). The large pore fractal dimensions and small structure factors indicate more pores widely dispersing in the soil, thus lower strength and stiffness.

The characteristics of the excess pore water pressure in CU triaxial tests are shown in Fig. 16. The excess pore water pressure increases with the strain and gradually stabilizes after growing to an asymptotic value. For CTC tests, the pore water pressure is constant positive at different confining pressures, reaching more than 90% of the peak value at the 1% strain. For RTC tests, when the confining pressure is 50 kPa, 100 kPa, and 150 kPa, the pore water pressure is negative and decreases with the strain. Only when the confining pressure is 200 kPa, the pore water pressure is positive, which first increases to a peak, then decreases slowly with increasing strain, and finally tends to be stable. This indicates that the volumetric expansion trend of soil specimens occurred under low confining pressure in RTC tests. However, the

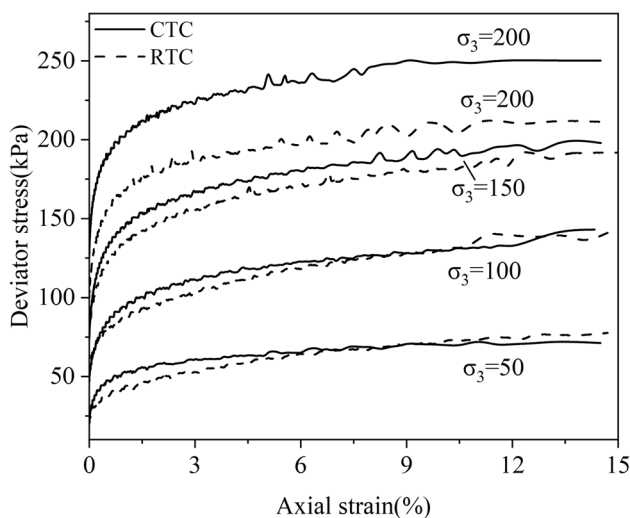


Fig. 14 Deviator stress–strain curves of soft clay ( $\sigma_3$ /kPa)

tendency is curbed when the confining pressure reaches a relatively high value. A similar volume response of soil specimens under RTC paths also has been found by Jiang et al. (2011) and Su et al. (2012). Notably, pore water pressure curves in RTC tests are similar at confining pressures of 50 kPa and 100 kPa. A reasonable explanation is that both natural structure and confining pressure can restrain soil expansion, which means the pore water pressure under RTC paths will not be negative if the inhibition is potent. As a result, the two-pore pressure curves under

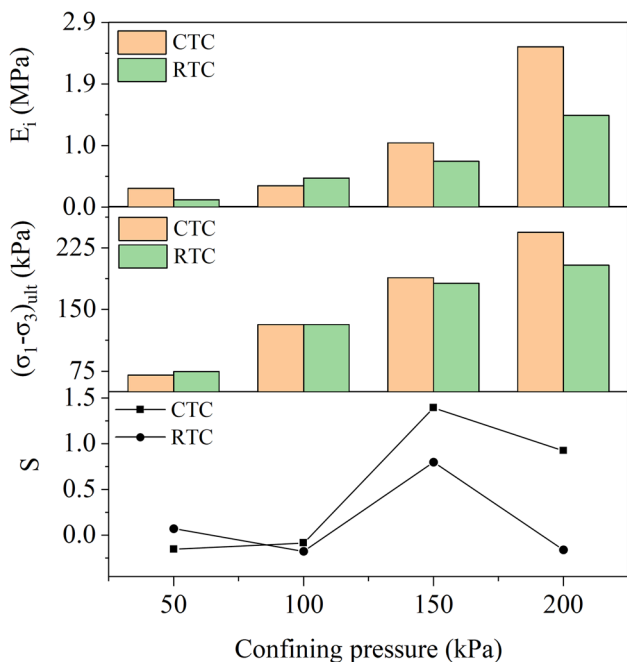


Fig. 15 Evolution of macro and micro parameters under different stress paths

50 kPa and 100 kPa exhibit a high degree of resemblance, which could attribute to the influence of natural structure. Although the natural structure is damaged when the confining pressure reaches 200 kPa, it is large enough to limit the specimen from dilation, making the pore pressure constantly positive.

### Microstructure evolution mechanisms influenced by the natural structure and stress paths

According to the findings of this investigation, different initial structural states have a significant effect on the macro and micro properties of the soil during shear. Figure 17a depicts the microstructure properties of idealized soft clay before and after  $K_0$  consolidation tests. Figure 17b indicates that the natural skeleton of the soil remains intact basically, and there is no noticeable difference compared to the natural soil, only a small height variation  $\nabla h_1$  emerged at the low consolidation pressure (lower than the preconsolidation pressure). However, when the applied consolidation pressure is higher than the preconsolidation pressure, the natural structure of soils is gradually damaged, as shown in Fig. 17c. The soil skeleton is compressed and gradually transformed from the previous flocculent structure to the dispersed structure, as manifested by the gradual breaking and disintegration of large aggregates and the degradation of interparticle cementation. As a result, when the confining pressure is 50 kPa and 100 kPa, the soil has considerable initial structural resistance due to big aggregates and strong cementation between particles. Even though the stress paths differ, soil specimens exhibit similar microstructure after shearing, as shown in Fig. 17d. When the natural structure of the soil is damaged ( $\sigma_3 = 150$  kPa and 200 kPa), the aggregates disintegrate and become smaller; a large amount of cementations

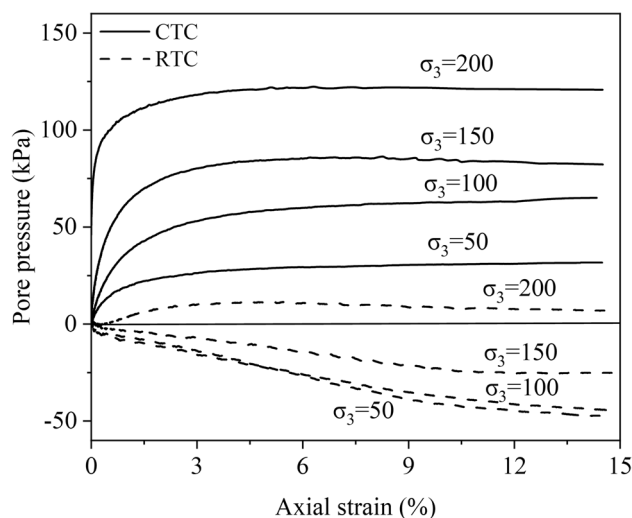
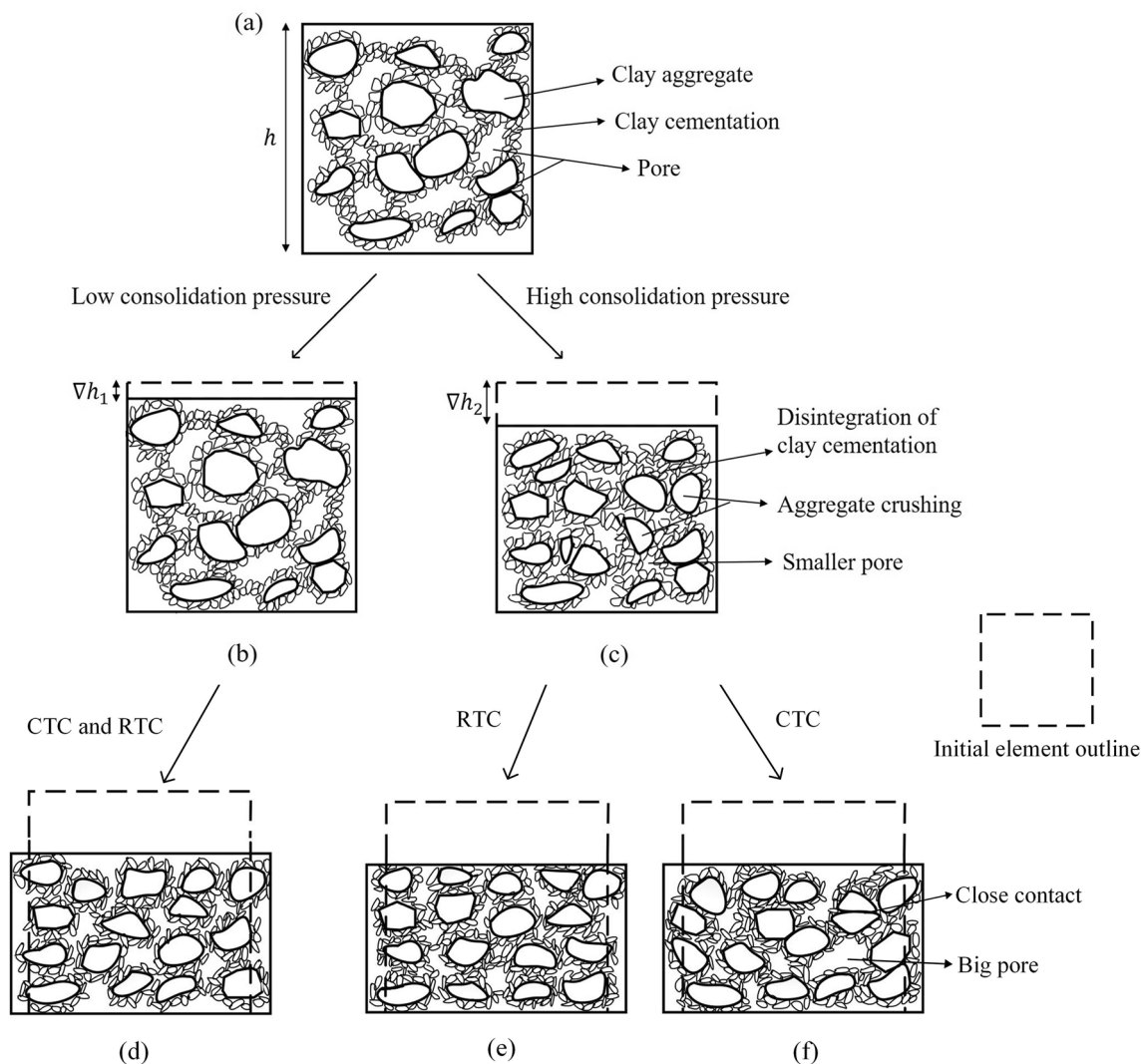


Fig. 16 Curves of pore pressure under different stress paths ( $\sigma_3$ /kPa)

breakage makes the force chains formed by particle contact smaller (Ng et al. 2020), which facilitates slip between particles, especially under RTC path. Figure 17e, f shows the microstructure characteristics after shear failure when the confining pressure exceeds the preconsolidation pressure. Some soil particles are in close contact with each other in CTC tests, and internal pores converge to generate a few big pores that are randomly scattered throughout the soil, resulting in an uneven distribution of pores and particles in specimens, as shown in Fig. 17f. For RTC tests, however, the soil structure is relatively homogeneous after shearing. The number of big pores is relatively few, leading to a broader distribution of pores (because the total volume of pores is constant), and the contact between soil particles is looser than in CTC tests. From the above analysis, it is explicit that

when the natural structure of the soft clay is strongly damaged after consolidation, the microstructure evolves toward relatively different failure patterns, i.e., loose uniform failure pattern for RTC specimens and locally dense non-uniform failure pattern for CTC specimens. In comparison, the contact between soil particles is weakened to a greater extent for the loose uniform failure pattern. Accordingly, the strength and stiffness of soil under RTC paths are significantly lower than those under CTC paths.

To the best of the authors' knowledge, prior studies either explore the structural effect of undisturbed soil (Kantesaria and Sachan 2022; Wang et al. 2021b) or focus on the influence of different stress paths (Bian et al. 2022; Zhou et al. 2020). Nevertheless, none of these studies investigated consolidation and shear as a unified process to consider the



**Fig. 17** Microstructural evolutionary characteristics of soft clay: **a** undisturbed natural structure; **b** after  $K_0$  consolidation under low confining pressure; **c** after  $K_0$  consolidation under high confining pres-

sure; **d** after shearing under low confining pressure; **e** after shearing under high confining pressure in CTC tests; **f** after shearing under high confining pressure in RTC tests

effect of structural damage caused by consolidation pressure on the subsequent mechanical behavior of soils. For sure, some research works are related to this study. Jiang et al. (2014) compared the microstructure of undisturbed and remolded specimens, pointing out that cementation bonds play a vital role in affecting the mechanical response of soil under different stress paths. Five particle orientation modes were suggested by Gao et al. (2020) to characterize microstructure evolution characteristics of remolded clays in different load stress paths. However, these studies did not consider the influence of natural structure damage on the mechanical behavior of undisturbed soil under different stress paths. In this study, the mechanical behavior of soil under the joint influence of natural structure and stress path has been purposely investigated. Results show that the specimens under RTC paths gradually show worse mechanical performance than CTC ones with the aggravation of natural structure damage.

## Conclusions

A series of  $K_0$  consolidation triaxial tests were performed on natural soft clay under different stress paths. FESEM and MIP tests on specimens before and after triaxial tests characterize the evolution of the soil microstructure. The influence of the natural structure of soft clay on its macro and micro characteristics under different stress paths is discussed in detail. Based on the above experimental research results, the following conclusions can be put forward:

- A new parameter termed the pore size distribution index was proposed based on MIP test results to quantify the microstructural characteristics of soft clay. It adequately considers the size distribution and volume effects of pore populations within the soil. This parameter therefore is superior to the conventional void ratio, which only reflects the global volume characteristics of pores when characterizing the soil structure.
- The damage variable determined based on pore size distribution indexes can evaluate the damage degree of the natural structure after  $K_0$  consolidation. When the confining pressure is less than the preconsolidation pressure (119 kPa), the natural structure of soils is slightly damaged after consolidation, with damage variables being only 0~0.1. However, damage variables reach 0.5~0.6 when the confining pressure range from 150 to 250 kPa.
- The difference in soil mechanical properties resulting from stress paths is closely related to the damage to the natural structure. The stress–strain and strength characteristics in CTC and RTC tests are similar when the natural structure is slightly damaged and vice versa. For example, at confining pressures of 50 kPa and 200 kPa, the difference in ultimate deviator stress between CTC and RTC tests is 6% and 20%, respectively.
- Once the natural structure is evidently damaged after consolidation, the soil microstructure develops in relatively different failure modes under the two stress paths. Loose uniform failure mode for RTC specimens and locally dense non-uniform failure mode for CTC specimens were put forward, in which the loose uniform failure pattern would weaken the macro mechanical properties of the soft clay to a greater extent.

**Funding** This work was supported by the National Natural Science Foundation of China (No. 41572255) and the Guangdong Provincial Key Laboratory of Modern Civil Engineering Technology (No. 2021B1212040003).

**Data availability** All data, models, and code generated or used during the study appear in the submitted article.

## Declarations

**Conflict of interest** The authors declare no competing interests.

## References

- Akbarimehr D, Eslami A, Aflaki E, Imam R (2020) Using empirical correlations and artificial neural network to estimate compressibility of low plasticity clays. *Arabian J Geosci* 13:1–11. <https://doi.org/10.1007/s12517-020-06228-3>
- Akbarimehr D, Eslami A, Imam R (2021) Correlations between compression index and index properties of undisturbed and disturbed Tehran clay. *Geotech Geol Eng* 39(7):5387–5393. <https://doi.org/10.1007/s10706-021-01821-z>
- Bian S, Mi Z, Li G, Ai Y, Du G (2022) Unified modeling behavior of rockfill materials along different loading stress paths. *Soils Found* 62(3):101155. <https://doi.org/10.1016/j.sandf.2022.101155>
- Cai YQ, Hao BB, Gu C, Wang J, Pan LY (2018) Effect of anisotropic consolidation stress paths on the undrained shear behavior of reconstituted Wenzhou clay. *Eng Geol* 242:23–33. <https://doi.org/10.1016/j.enggeo.2018.05.016>
- Cui ZD, Yang JQ, Yuan L (2015) Land subsidence caused by the interaction of highrise buildings in soft soil areas. *Nat Hazard* 79:1199–1217. <https://doi.org/10.1007/s11069-015-1902-8>
- Delage P (2010) A microstructure approach to the sensitivity and compressibility of some Eastern Canada sensitive clays. *Géotechnique* 60(5):353–368. <https://doi.org/10.1680/geot.2010.60.5.353>
- Du JP, Zhou AN, Shen SL, Bu YH (2022) Fractalbased model for maximum penetration distance of grout slurry flowing through soils with different dry densities. *Comput Geotech* 141:104526. <https://doi.org/10.1016/j.compgeo.2021.104526>
- Eslami A, Akbarimehr D (2021) Failure analysis of clay soilrubber waste mixture as a sustainable construction material. *Constr Build Mater* 310:125274. <https://doi.org/10.1016/j.conbuildmat.2021.125274>
- Gao QF, Hattab M, Jrad M, Fleureau JM, Hicher PY (2020) Microstructural organization of remoulded clays in relation with dilatancy/contractancy phenomena. *Acta Geotech* 15:223–243. <https://doi.org/10.1007/s11440-019-00876-w>

- Gasparre A, Coop MR (2008) Quantification of the effects of structure on the compression of a stiff clay. *Can Geotech J* 45(9):1324–1334. <https://doi.org/10.1139/t08-052>
- Gasparre A, Nishimura S, Coop MR, Jardine RJ (2011) The influence of structure on the behaviour of London Clay. *Stiff Sedimentary Clays: Genesis and Engineering Behaviour: Géotechnique Symposium in Print 2007*. Thomas Telford Ltd. pp 67–79 <https://doi.org/10.1680/ssc.41080.0007>
- GB, T 50123–2019 (2019) Standard for soil test method. China Planning Press, Beijing (in Chinese)
- Guglielmi S, Cotecchia F, Cafaro F, Gens A (2022) Analysis of the micro to macro response of clays to compression. *Géotechnique* 1–21. <https://doi.org/10.1680/jgeot.21.00233>
- He YQ, Wang S, Liao HJ, Wu W (2022) A hypoplastic constitutive model for structured soils. *Comput Geotech* 151:104935. <https://doi.org/10.1016/j.compgeo.2022.104935>
- Jiang MJ, Hu HJ, Peng JB, Leroueil S (2011) Experimental study of two saturated natural soils and their saturated remoulded soils under three consolidated undrained stress paths. *Front Archit Civ Eng China* 5:225–238. <https://doi.org/10.1007/s11709-011-0108-8>
- Jiang MJ, Zhang FG, Hu HJ, Cui YJ, Peng JB (2014) Structural characterization of natural loess and remolded loess under triaxial tests. *Eng Geol* 181:249–260. <https://doi.org/10.1016/j.enggeo.2014.07.021>
- Kantesaria N, Sachan A (2022) Smallstrain shear modulus and yielding characteristics of compacted highplasticity clay. *Géotechnique* 72(5):424–437. <https://doi.org/10.1680/jgeot.20.p.089>
- Kondner RL (1963) Hyperbolic stress-strain response: cohesive soils. *J Geotech Geoenviron Eng* 89(1):115–143. <https://doi.org/10.1061/jsfeaq.0000479>
- Korvin G (1992) *Fractal models in the earth sciences*. Elsevier, Amsterdam
- Lei XY (1988) The types of loess pores in China and their relationship with collapsibility. *Sci Sin Ser B Chem Biol Agric Med Earth Sci* 31(11):1398–1410. <https://doi.org/10.1111/j.1755-6724.1989.mp2004008.x>
- Lei HY, Liu M, Jiang Y, Sun XF (2020) Deformation of Tianjin soft clay and corresponding micromechanism under cyclic loading. *Can Geotech J* 57(12):1893–1902. <https://doi.org/10.1139/cgj-2019-0352>
- Li J, Tang YQ, Feng W (2020a) Creep behavior of soft clay subjected to artificial freeze–thaw from multiplescale perspectives. *Acta Geotech* 15:2849–2864. <https://doi.org/10.1007/s11440-020-00980-2>
- Li P, Shao SJ, Vanapalli SK (2020b) Characterizing and modeling the poresize distribution evolution of a compacted loess during consolidation and shearing. *J Soils Sediments* 20:2855–2867. <https://doi.org/10.1007/s11368-020-02621-3>
- Li P, Shao SJ, Xiao T, Zhu DD (2021) Poresize distribution evolution of intact, compacted, and saturated loess from China during consolidation and shearing. *Adv Civ Eng* 1–14. <https://doi.org/10.1155/2021/6644471>
- Liu HB, Sun S, Wang LX, Zhang YL, Wang J, Luo GB, Han LL (2020) Microscopic mechanism of the macroscopic mechanical properties of cement modified subgrade Silty soil subjected to freezethaw cycles. *Appl Sci* 10(6):2182. <https://doi.org/10.3390/app10062182>
- Liu WH, Zhang HY, Li WG, Kong GQ, Lin XY (2022) An advanced critical state constitutive model for overconsolidated structured soils. *Int J Geomech* 22(5):06022004. [https://doi.org/10.1061/\(asce\)gm.1943-5622.0002349](https://doi.org/10.1061/(asce)gm.1943-5622.0002349)
- Low HE, Phoon KK (2008) Effect of cementation on the compressibility of Singapore upper marine clay. *Can Geotech J* 45(7):1018–1024. <https://doi.org/10.1139/t08-030>
- Ma PF, Wang WX, Zhang BW, Wang JL, Shi GS, Huang GQ, Chen FL, Jiang LM, Lin H (2019) Remotely sensing largeand smallscale ground subsidence: a case study of the Guangdong-Hong Kong–Macao Greater Bay Area of China. *Remote Sens Environ* 232:111282. <https://doi.org/10.1016/j.rse.2019.111282>
- Musso G, Azizi A, Jommi C (2020) A microstructure-based elastoplastic model to describe the behaviour of a compacted clayey silt in isotropic and triaxial compression. *Can Geotech J* 57:1025–1043. <https://doi.org/10.1139/cgj-2019-0176>
- Nan JJ, Peng JB, Zhu FJ, Ma PH, Liu R, Leng YQ, Meng ZJ (2021) Shear behavior and microstructural variation in loess from the Yan’an area, China. *Eng Geol* 280:105964. <https://doi.org/10.1016/j.enggeo.2020.105964>
- Ng CWW, Akinniyi DB, Zhou C (2020) Influence of structure on the compression and shear behaviour of a saturated lateritic clay. *Acta Geotech* 15:3433–3441. <https://doi.org/10.1007/s11440-020-00981-1>
- Ovando Shelley E, Rodríguez Rebolledo JF, ValderramaAtayupanqui YV (2020) Geotechnical characteristics of natural and reconstituted lacustrine Mexico City clays. *Geotech Geol Eng* 38:1471–1484. <https://doi.org/10.1007/s10706-019-01103-9>
- Qiao YS, Liu JG, Cao L, Khan MHR, Xu XD, Tan L (2021) Contribution of continuously stable sediment input to the formation of the Pearl River delta since the middle Holocene. *Quat Int* 598:7889. <https://doi.org/10.1016/j.quaint.2021.05.010>
- Ren YB, Yang SL, Zhang SX, Yang Q, Wang Y, He B, Huan CY (2022) Experimental study of the thixotropic strength recovery and microstructural evolution of marine clays. *J Geotech Geoenviron Eng* 148(8):04022059. [https://doi.org/10.1061/\(asce\)gt.1943-5606.0002833](https://doi.org/10.1061/(asce)gt.1943-5606.0002833)
- Romero E, Simms PH (2008) Microstructure investigation in unsaturated soils: a review with special attention to contribution of mercury intrusion porosimetry and environmental scanning electron microscopy. *Geotech Geol Eng* 26:705–727. [https://doi.org/10.1007/978-1-4020-8819-3\\_8](https://doi.org/10.1007/978-1-4020-8819-3_8)
- Su SQ, Deng BT, Hou JF, Lv Z (2012) Experimental study on shear strength of intact loess at different stress paths. *Advanced Materials Research. Trans Tech Publ*, pp 2891–2894
- Sun H, Mašin D, Najser J, Neděla V, Navrátilová E (2020) Fractal characteristics of pore structure of compacted bentonite studied by ESEM and MIP methods. *Acta Geotech* 15:1655–1671. <https://doi.org/10.1007/s11440-019-00857-z>
- Tan Y, Jiang WZ, Rui HS, Lu Y, Wang DL (2020) Forensic geotechnical analyses on the 2009 buildingoverturning accident in Shanghai, China: beyond common recognitions. *J Geotech Geoenviron Eng* 146(7):05020005. [https://doi.org/10.1061/\(asce\)gt.1943-5606.0002264](https://doi.org/10.1061/(asce)gt.1943-5606.0002264)
- Wang YH, Xu D (2007) Dual porosity and secondary consolidation. *J Geotech Geoenviron Eng* 133(7):793–801. [https://doi.org/10.1061/\(asce\)1090-0241\(2007\)133:7\(793\)](https://doi.org/10.1061/(asce)1090-0241(2007)133:7(793))
- Wang JD, Li P, Ma Y, Vanapalli SK, Wang XG (2020) Change in poresize distribution of collapsible loess due to loading and unloading. *Acta Geotech* 15:1081–1094. <https://doi.org/10.1007/s11440-019-00815-9>
- Wang HL, Sun H, Huang ZX, Ge XR (2021a) A microstructural investigation on hydraulic conductivity of soft clay. *Bull Eng Geol Environ* 80:4067–4078. <https://doi.org/10.1007/s10064-021-02176-8>
- Wang Y, Yang H, Jing X (2021b) Structural characteristics of natural loess in Northwest China and its effect on shear behavior. *Geotech Geol Eng* 39:65–78. <https://doi.org/10.1007/s10706-020-01420-4>
- Washburn EW (1921) The dynamics of capillary flow. *Phys Rev* 17(3):273–283. <https://doi.org/10.1103/PhysRev.17.273>
- Xu L, Coop MR (2016) Influence of structure on the behavior of a saturated clayey loess. *Can Geotech J* 53(6):1026–1037. <https://doi.org/10.1139/cgj-2015-0200>
- Yin PH, Vanapalli SK (2022) Model for predicting evolution of microstructural void ratio in compacted clayey soils. *Can Geotech J* 59(9):1602–1621. <https://doi.org/10.1139/cgj-2021-0057>

- Zeng LL, Ji F, Wang H, Cai YQ, Hong ZS (2022) Estimating hydraulic conductivity of naturally sedimented clays using compression curves. *Acta Geotech* 17:1815–1827. <https://doi.org/10.1007/s11440-021-01306-6>
- Zhang YZ, Zuo SY, Li RYM, Mo YC, Yang GS, Zhang M (2020) Experimental study on the mechanical properties of Guiyang red clay considering the meso micro damage mechanism and stress path. *Sci Rep* 10(1):17449. <https://doi.org/10.1038/s41598-020-72465-x>
- Zhang XW, Liu XY, Xu YQ, Wang G, Ren YB (2023) Compressibility, permeability and microstructure of finegrained soils containing diatom microfossils. *Géotechnique* 1–15. <https://doi.org/10.1680/jgeot.22.00155>
- Zheng YM, Sun H, Hou MX, Ge XR (2021) Microstructure evolution of soft clay under consolidation loading. *Eng Geol* 293:106284. <https://doi.org/10.1016/j.enggeo.2021.106284>
- Zheng Y, Baudet BA, Delage P, Pereira JM, Sammonds P (2022) Pore changes in an illitic clay during one-dimensional compression. *Géotechnique* 1–16. <https://doi.org/10.1680/jgeot.21.00206>
- Zhou ZW, Ma W, Zhang SJ, Mu YH, Li GY (2020) Experimental investigation of the pathdependent strength and deformation behaviours of frozen loess. *Eng Geol* 265:105449. <https://doi.org/10.1016/j.enggeo.2019.105449>

Springer Nature or its licensor (e.g. a society or other partner) holds exclusive rights to this article under a publishing agreement with the author(s) or other rightsholder(s); author self-archiving of the accepted manuscript version of this article is solely governed by the terms of such publishing agreement and applicable law.